Morphology-controlled synthesis and a comparative study of the physical properties of SnO_2 nanostructures: from ultrathin nanowires to ultrawide nanobelts

2009 Nanotechnology 20 135605

(http://iopscience.iop.org/0957-4484/20/13/135605)

Nanotechnology **20** (2009) 135605 (8pp) doi:10.1088/0957-4484/20/13/135605

Morphology-controlled synthesis and a comparative study of the physical properties of SnO_2 nanostructures: from ultrathin nanowires to ultrawide nanobelts

Z Zhang[1], J Gao[1], L M Wong[2], J G Tao[1], L Liao[1], Z Zheng[1], G Z Xing[1], H Y Peng[1], T Yu[1], Z X Shen[1], C H A Huan[1], S J Wang[2] and T Wu[1,3]

[1] Division of Physics and Applied Physics, School of Physical and Mathematical Sciences, Nanyang Technological University, 637371, Singapore
[2] Institute of Materials Research and Engineering, 3 Research Link, 117602, Singapore

E-mail: tomwu@ntu.edu.sg

Received 22 December 2008, in final form 27 January 2009
Published 11 March 2009
Online at stacks.iop.org/Nano/20/135605

Abstract
Controlled synthesis of one-dimensional materials, such as nanowires and nanobelts, is of vital importance for achieving the desired properties and fabricating functional devices. We report a systematic investigation of the vapor transport growth of one-dimensional SnO_2 nanostructures, aiming to achieve precise morphology control. SnO_2 nanowires are obtained when SnO_2 mixed with graphite is used as the source material; adding TiO_2 into the source reliably leads to the formation of nanobelts. Ti-induced modification of crystal surface energy is proposed to be the origin of the morphology change. In addition, control of the lateral dimensions of both SnO_2 nanowires (from ∼15 to ∼115 nm in diameter) and nanobelts (from ∼30 nm to ∼2 μm in width) is achieved by adjusting the growth conditions. The physical properties of SnO_2 nanowires and nanobelts are further characterized and compared using room temperature photoluminescence, resonant Raman scattering, and field emission measurements.

(Some figures in this article are in colour only in the electronic version)

1. Introduction

Tin dioxide (SnO_2) is a versatile wide-band-gap ($E_g = 3.62$ eV at 300 K for bulk SnO_2) n-type semiconductor with potential applications in electronic, optoelectronic, gas sensing, and energy generation devices. One-dimensional (1D) SnO_2 nanomaterials like nanowires (NWs), nanobelts (NBs), and more complex hierarchical nanostructures have attracted great interest in recent years due to their promising performances in nanoscale functional devices [1–19]. Various approaches have been carried out to fabricate SnO_2 nanomaterials, such as the molten salt method [17, 20, 21], laser ablation vapor deposition [22, 23], hydrothermal method [24], and plasma treatment [16]. Among them, vapor transport growth is one of the most widely used methods due to its low cost and high flexibility. Different source precursors such as Sn [14, 25–31], SnO [32–38], SnO_2 [13, 32], SnO + graphite [39], and SnO_2 + graphite [40–43] have been used in previous studies.

Although high-performance devices based on individual NWs or NBs have already been demonstrated, many questions related to the mechanisms of nanomaterial growth remain to be addressed. In particular, precise control on the morphology and the dimension of 1D nanomaterials is one of the obstacles researchers have to overcome in order to achieve desired and uniform performances in nanomaterial-based devices. SnO_2 is one of the most investigated oxide nanomaterials, and different 1D morphologies have been reported [36, 41, 44–46]. For example, by evaporating Sn powder, Luo *et al* synthesized SnO_2 NWs and NBs at 850 °C and 1000 °C, respectively [26]. Wang *et al* acquired SnO_2 NWs, NBs, and nanotubes by

[3] Author to whom any correspondence should be addressed.

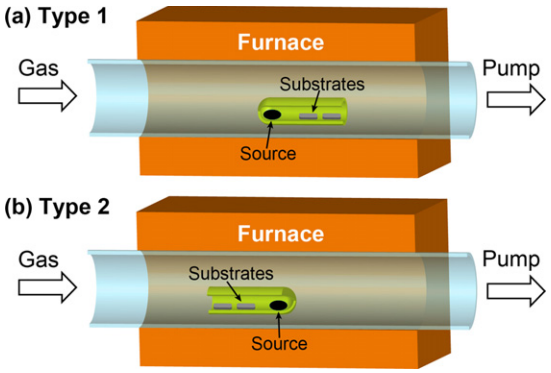

Figure 1. Schematic illustration of the experimental setups. (a) Type 1: the quartz tube opens toward the downstream direction. (b) Type 2: the quartz tube opens toward the upstream direction.

adjusting the source material, temperature, and pressure [44]. Lilach *et al* showed that the NW growth direction could be controlled by modulating the flow rate of the carrier gas [47]. The choice of catalyst metals also affects the morphologies and sizes of the growth products [39, 48]. However, reproducible synthesis of 1D SnO_2 nanomaterials with controlled morphology and tunable dimensions still remains challenging.

In this study on the growth of 1D SnO_2 nanomaterials, we found that a dramatic morphology change from NW to NB can be induced by adding TiO_2 to the source powder. We investigated the vapor transport growth of SnO_2 in detail and compared the impact of various growth parameters. Further to the previous studies, adding TiO_2 into the source powder gives us an additional degree of freedom to achieve the selective growth of SnO_2 NBs and NWs. Although the Ti doping level is very low and cannot be determined by the experimental techniques accessible to us, the surface-orientation-dependent energy modification appears to the origin of the morphology change. Furthermore, the lateral sizes of both NWs and NBs were tailored in wide ranges by adjusting the experimental conditions. Finally, as a consequence of their different morphologies, SnO_2 NWs and NBs show different optical and field emission properties.

2. Experiments

SnO_2 1D nanostructure fabrication was conducted by using a vapor transport method. The growth took place in a Carbolite three-zone horizontal tube furnace equipped with gas supplying and pumping systems. The schematic drawings of two typical experiment setups, named type 1 and type 2, respectively, are shown in figures 1(a) and (b). To prepare the source powder for the NW growth, SnO_2 was mixed with graphite (weight ratio 1:1) and ground in an agate mortal for 30 min. For the NB growth, SnO_2 was mixed with TiO_2 and graphite (weight ratio 1:1:2). The source powder was placed at the end of a quartz test tube (diameter $d = 1$, length $L = 15$ cm). Si(111) wafers coated with 4 nm Au films with a dimension of 6 mm × 8 mm were used as the growth substrates and were placed near the open end of the quartz tube. The quartz tube was then inserted into the tube furnace with the source located at the furnace center and with the open end pointing either downstream (type 1) or upstream (type 2). Ar mixed with O_2 was introduced as the carrier gas and the pressure was maintained at 20 mbar by controlled pumping. To start the growth, the temperature was ramped to 1100 °C at a rate of 20 °C min^{-1}. The substrate temperature was calibrated to be ∼800 °C. After growth for 1 h, white or light gray products were observed on the Si substrates.

Table 1. Comparison of experimental parameters and results.

Sample No.	Tube orientation	Carrier gas		Morphology	Size[a]
# 1	Type 1	O_2 (0.05%)	100 sccm	NW	15.3 nm
# 2	Type 2	O_2 (0.05%)	500 sccm	NW	66.6 nm
# 3	Type 2	O_2 (5%)	30 sccm	NW	113 nm
# 4	Type 2	O_2 (5%)	30 sccm	NB	33.6 nm
# 5	Type 2	O_2 (100%)	200 sccm	NB	114 nm
# 6	Type 2	O_2 (100%)	1000 sccm	NB	1.7 μm

[a] Size indicates the average diameter for NWs and the average width for NBs.

The morphology and the crystalline structure of the as-fabricated SnO_2 nanostructures were characterized with a JEOL JSM-6700F field emission scanning electron microscope (FESEM) and a JEOL 2100 high-resolution transmission electron microscope (TEM), both equipped with electron energy-dispersive x-ray (EDX) spectrometers. X-ray powder diffraction (XRD) patterns were recorded on a Bruker D8 Advanced diffractometer using Cu Kα radiation. X-ray photoelectron spectroscopy (XPS) measurements were made using a VG ESCALAB 220i-XL system equipped with a monochromatic x-ray source. Photoluminescence (PL) properties were studied at room temperature (RT) using a continuous-wave He–Cd laser with a 325 nm wavelength. RT Raman measurements were performed on a WITEC CRM200 confocal Raman system with exciting wavelength of 532 nm. RT field emission (FE) measurements were carried out in a high vacuum (10^{-7} mbar) chamber. The distance between the anode and the surface of the emitting samples (cathode) was fixed at 100 μm and the current–voltage (I–V) curves were recorded using a Keithley 2400 source meter.

3. Results and discussion

3.1. SEM and TEM studies

Our initial intention of using a source of SnO_2 mixed with TiO_2 and graphite was to synthesize nanomaterials based on the isostructural system TiO_2–SnO_2, which may find applications in gas detection [49, 50]. However, as we will show later, the current synthesis method is not effective for doping Ti in SnO_2 due to the very low vapor pressure of Ti. Instead, this synthesis route allowed us to achieve a good morphology control on the SnO_2 nanomaterials. Table 1 provides a brief summary of the experimental parameters and the results of six typical experiments. SnO_2 mixed with graphite was used as the source powders to prepare samples # 1–3, while TiO_2 was added into the source for the growth of samples # 4–6.

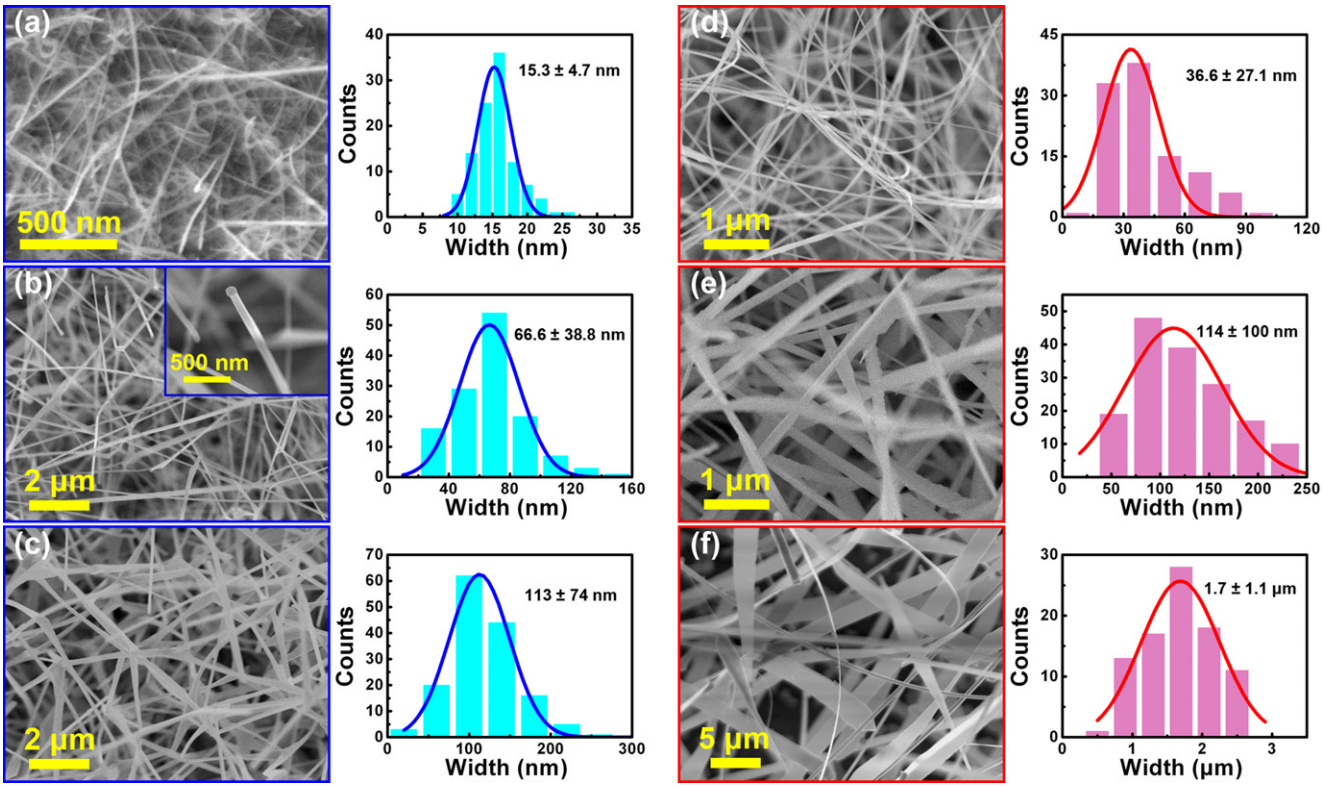

Figure 2. SEM images of SnO_2 NW samples # 1–3 ((a)–(c)) and NB samples # 4–6 ((d)–(f)). Also shown are the corresponding statistical distributions of NW diameter and NB width. The inset in (b) shows a spherical catalyst droplet on the NW tip. The experimental conditions are listed in table 1.

The correlations between adding TiO_2 in the source powder and the resulting nanostructure morphologies indicate a simple rule: adding TiO_2 leads to NBs; otherwise NWs form. The existence or absence of TiO_2 dictates the morphologies of the products, though the lateral sizes can be tailored by other growth parameters. No exception was observed in a total of over 50 experimental runs we conducted under different conditions of carrier gas (O_2: 0.05%–100%; flow rate: 30–1000 sccm; pressure: 10–50 mbar), of growth temperature (900–1100 °C), of the experimental setup (quartz tube with both ends open or one end sealed), and even in different tube furnaces (carbolite three-zone or Lindberg/Blue Mini-Mite horizontal tube furnace).

SEM images of NW samples # 1–3 and NB samples # 4–6 are shown in figure 2. The as-fabricated nanostructures are quite uniform in morphology and size. The NWs and NBs are quite long and are on the order of tens to hundreds of micrometers. The diameters of the NWs are highly tunable, and a clear incremental trend from sample # 1 to sample # 3 was observed. There are also dramatic increases of NB width from sample # 4 to sample # 6, while the NB thickness remains roughly unchanged and is in the range 20–50 nm. For each sample, the dimensions of more than 100 NWs or NBs were measured, and the statistical results were plotted in the histograms in figure 2. By Gaussian fitting, the NW diameters of samples # 1–3 were determined to be 15.3 ± 4.7, 66.6 ± 38.8, and 113 ± 74 nm, respectively. The NB widths of samples # 4–6 were estimated to be 36.6 ± 27.1, 114 ± 100 nm, and 1.7 ± 1.1 μm, respectively. Thus we are able to tune the dimension of the 1D SnO_2 nanomaterials over almost two orders of magnitude.

The oxygen partial pressure appears to be a key parameter: generally, a higher O_2 partial pressure favors the growth of thicker NWs and wider NBs. We can also tell from table 1 that the growth of SnO_2 NBs normally requires a higher oxygen pressure than for growth of NWs. In the SnO_2 NB sample # 6, the width-to-thickness ratio reaches 100, which, to the best of our knowledge, is the highest ever reported for SnO_2 nanobelts. A substantial fraction of the NBs are wider than 2 μm, which is among the widest belt-like oxide and chalcogenide nanomaterials reported in the literature [51–53]. The dimensions of most NWs are smaller than the critical value of 90 nm, which is consistent with the calculation by Wang *et al* [46]. However, the width of the narrowest NBs in sample # 4 also falls into this range, and this contradiction may stem from the surface energy modification induced by Ti.

It is often difficult to determine the exact growth mechanism of 1D nanostructures due to a lack of *in situ* observation. In most cases, there is a competition between vapor–liquid–solid (VLS) and vapor–solid (VS) mechanisms, and their balance is modified by very subtle changes of growth conditions [48]. Control experiments showed that no NW or NB would grow on Si substrates without the coating of a Au film. However, careful SEM investigations suggest that the growth of SnO_2 NWs and NBs deviates from the conventional VLS mechanism. As shown in the inset in figure 2(b), spherical particles, which were determined to be pure Sn by EDX analysis, were observed on most of the NW tips, indicating

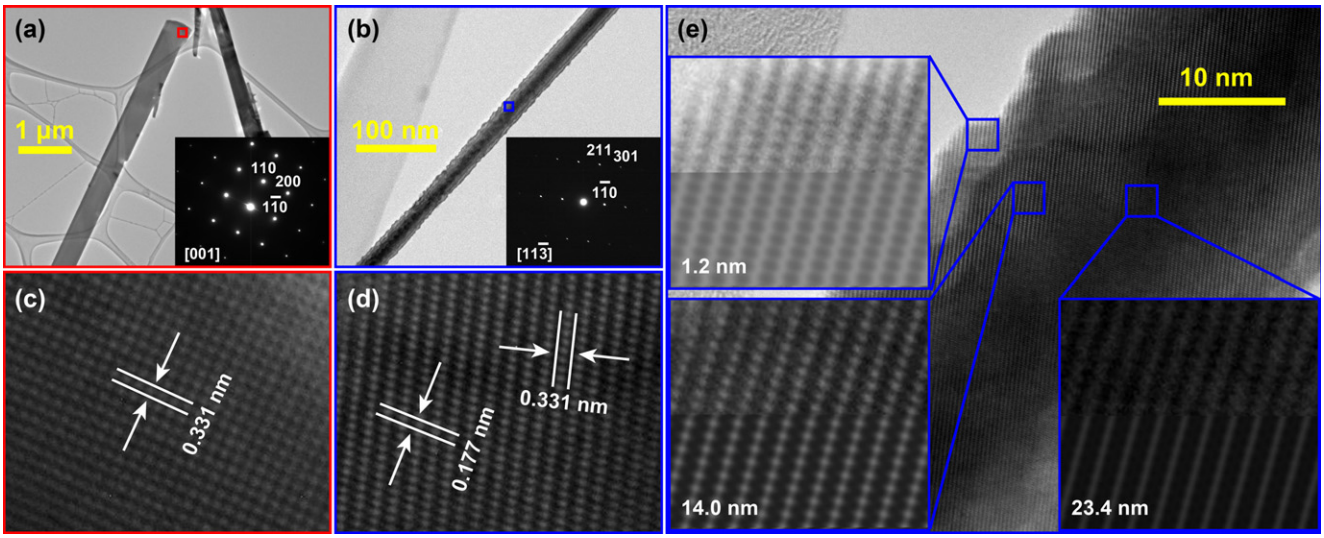

Figure 3. TEM images of a SnO_2 NB (a) and a SnO_2 NW (b) with the corresponding SAED patterns as insets. ((c), (d)) HRTEM images taken at the marked areas in (a) and (b), respectively. (e) HRTEM image of the NW in (b). The insets show comparisons between the magnified images (upper half) and the simulated patterns (lower half) at three specified positions.

a self-catalytic VLS dominated growth mechanism [34]. Such Sn particles were not found on the NBs; thus the growth of NBs is likely dominated by the VS mechanism.

The structures of the as-grown materials were further analyzed in a TEM operating at 200 kV. Low-resolution TEM images are shown in figures 3(a) and (b). The lacey carbon film under the NBs can be clearly observed, indicating that the NBs are quite thin. The side boundaries of the NBs are very smooth and they show uniform thickness. In contrast, the NWs show rough surfaces and their thickness decreases from the centers to the boundaries. The selected area electron diffraction (SAED) data in the insets indicate that the growth direction of the NBs is [110]. The growth of NWs is more complex: the direction is close to [302] with the axial growth plane being (301). The SAED patterns show no sign of secondary phase and support a pure rutile structure for both NBs and NWs. The HRTEM images of the NB and the NW at the selected areas are shown in figures 3(c) and (d), respectively. No structural defect was observed, indicating a single-crystalline nature. The planes with interplanar d-spacings 0.331 and 0.177 nm can be indexed as {110} and {211}, respectively. The HRTEM results are consistent with the SAED patterns, and confirm the tetragonal rutile structure for both NWs and NBs.

To further study the morphology of the NWs, an HRTEM simulation on rutile SnO_2 was performed using JEMS software with the observation direction along [11$\bar{3}$]. By comparing the simulated images with the experimental HRTEM data, we determined the thickness at a few selected positions on the NW. Similar procedures have previously been used to determine the local thickness of ZnO NBs [54]. As shown in the insets of figure 3(e), the good matching between the experimental images (upper half) and the simulated ones (lower half) allowed us to determine the local thickness to be 1.2, 14.0, and 23.4 nm at the selected positions. Considering these data along with the NW diameter of ∼25 nm, we conclude that the cross section of the NWs is close to a circle. Thus the NW is not a retrogressed NB with the aspect ratio reduced to 1. Otherwise it would show a rectangular or a square-shaped cross section.

3.2. XRD and XPS studies

We carried out additional characterizations on the NW and NB samples. Unless otherwise stated, the NWs and NBs used in the experiments refer to sample # 1 and sample # 6, respectively. Sample # 1 represents the thinnest NWs and sample # 6 the widest NBs. The XRD patterns of the NW and NB samples are shown in figure 4(a). Both of them show a tetragonal rutile SnO_2 structure with lattice constants $a = 0.4737$ and $c = 0.3186$ nm. The NB pattern shows a higher (110) peak intensity than that of the NWs, consistent with their growth direction of [110] as determined in the TEM observation. As shown in figure 4(b), a weak Sn (200) peak appears only in the NW data. This peak comes from the Sn catalyst droplets on the NW tips, consistent with the SEM observations shown in figure 2(b).

The NW and NB samples show very similar XPS results. As shown in figure 4(d), full range surveys on both NW and NB samples did not detect any peak related to Ti. A detailed scan from 470 to 455 eV also showed no sign of Ti_{2p} peak. Therefore, the Ti doping level is lower than the detection limit of XPS, i.e., 0.1%.

3.3. Mechanism of morphology control

The salient feature of this study is that adding TiO_2 to the source powder was found to induce a significant morphology change in the 1D SnO_2 nanomaterials. In equilibrium or quasiequilibrium growth, the shapes and dimensions of nanostructures are dictated by the differences of surface energies between various growth directions. The surface energies may be influenced by factors such as size effect, supersaturation state, unintentionally introduced impurities, and intentional doping. For example, based on experimental

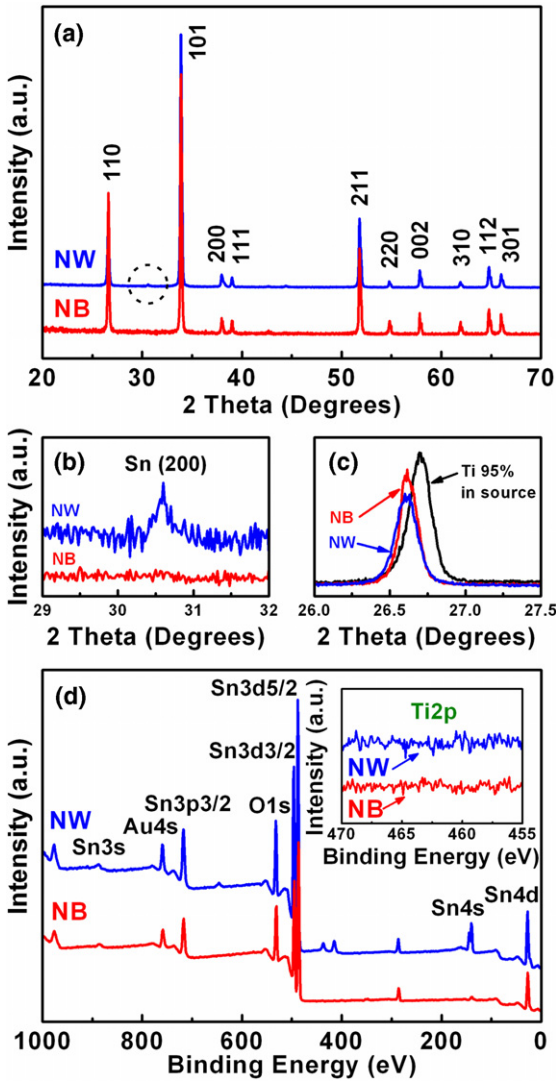

Figure 4. (a) XRD patterns of the SnO_2 NWs (sample # 1, upper curve) and the SnO_2 NBs (sample # 6, lower curve). The region marked by a dashed circle is magnified and shown in (b). (c) Detailed scan of the (110) peaks. The result of a control experiment with a higher Ti molar ratio (95%) in the source powder is shown as comparison. (d) XPS survey spectra of the SnO_2 NWs (sample # 1, upper curve) and the SnO_2 NBs (sample # 6, lower curve). Inset: no Ti_{2p} peak is seen in the high-resolution scans.

results and theoretical calculations, Wang *et al* concluded that undoped SnO_2 favors the NW morphology when the size is smaller than 90 nm while the NB morphology is preferred with larger sizes [46]. Our previous study on Cu-doped ZnO nanostructures [56] showed that a morphology change from NW to nanoneedle and nanonail can be induced by very subtle modifications of the growth environments.

The subtle energy balance between the various growth directions can be broken by minimal changes of composition or environment. In a previous study, Fan *et al* found that the growth of ZnO NWs (*c*-axial) and NBs (*a*-axial) was effectively controlled by indium doping [57, 58]. In another work, it was observed that NWs may change direction during growth to form zigzag-shaped structures because several groups of surfaces of rutile SnO_2 have similar energies [35, 59]. As shown in figure 2, we frequently observed branched nanowires. Similar phenomena have also been reported for pure SnO_2 NBs [60]. However, the growth direction rarely changes in the NB samples, which may indicate that sufficient energy differences are generated between various growth surfaces and the formation of NBs is stabilized.

Herein, we propose that Ti from the source powder modifies the surface energies of SnO_2, thus particular lateral growth directions are favored, leading to the anisotropic growth of NBs. Such dramatic changes of growth morphology are similar to the previous observations of conversion between ZnO NWs and NBs by In doping, which was accounted for by minimization of Gibbs free energy [57, 58]. However, we should note that Ti may not be doped significantly into the SnO_2 matrix even though its decoration on the growth surfaces modifies the surface energy and the morphology. The Ti ions decorating the surfaces may not be incorporated into the bulk effectively, which explains the fact that there is no obvious shift of the (220) peak in the XRD data of NBs shown in figure 4(c).

In our experiments, the vapor pressure of Ti at the growth temperature is quite low (even at 1660 °C it is only 0.49 Pa, and in contrast the vapor pressure of Zn reaches 19.2 Pa at 420 °C), causing the detection of Ti to be extremely difficult. This situation is different from the conventional polycrystal growth through solid state reactions where the structural analogy between TiO_2 and SnO_2 leads to the formation of a solid solution over a wide composition range above the spinodal decomposition temperature [50, 55]. In order to verify that Ti vapor does come out at the source temperature of 1100 °C, we carried out a control experiment by dramatically increasing the Ti molar content in the source powder. We found that Ti doping becomes much more detectable when the Ti content is high enough although the sample quality is compromised. As an example, figure 4(c) shows a detailed scan around the SnO_2 (110) peak for a case of 95% Ti in the source, which reveals a small peak shift of ∼0.1°, indicating a reduction of the lattice constant by ∼0.0015 nm. Since there is a linear relationship between lattice parameters and composition molar ratios in such solid solutions [55], it can be calculated that the Ti doping level in the control experiment is ∼10%. Therefore, we conclude that Ti vapor does exist under the experimental conditions used although the Ti concentration in the SnO_2 nanomaterials is lower than the detection limits of the XRD and XPS techniques.

To further investigate the effect of Ti doping, we tried to grow SnO_2 nanostructures on Si substrates coated with 10 nm Ti films. The growth parameters were kept the same as in sample # 3. As shown in figure 5(a), with the bare Ti film, the density of SnO_2 NWs is very low. On the other hand, as demonstrated in figure 5(b), dense SnO_2 NWs were grown if a 4 nm layer of Au was sputtered on top of the Ti-coated substrates. Therefore, there seemed to be minimal reaction between the Ti film and the SnO_2 nanowires, and doping from the Ti film is not as effective as from the TiO_2-mixed source powder, which may be a result of the lower temperature at the substrate position that the source temperature.

On the other hand, in order to study how general the doping effect is on the morphology, we carried out control

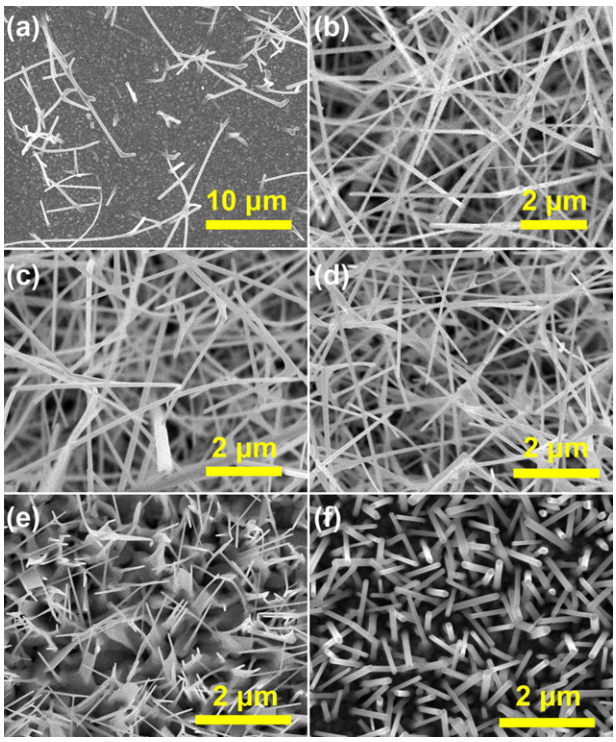

Figure 5. SnO_2 NWs grown on Ti-coated Si substrates without Au catalyst (a) and with Au catalyst (b). SnO_2 NWs synthesized with MnO_2 (c) or MgO (d) mixed in the source powders. (e) ZnO NWs fabricated with TiO_2 powder mixed in the source. (f) Pure ZnO NWs grown without TiO_2 in the source.

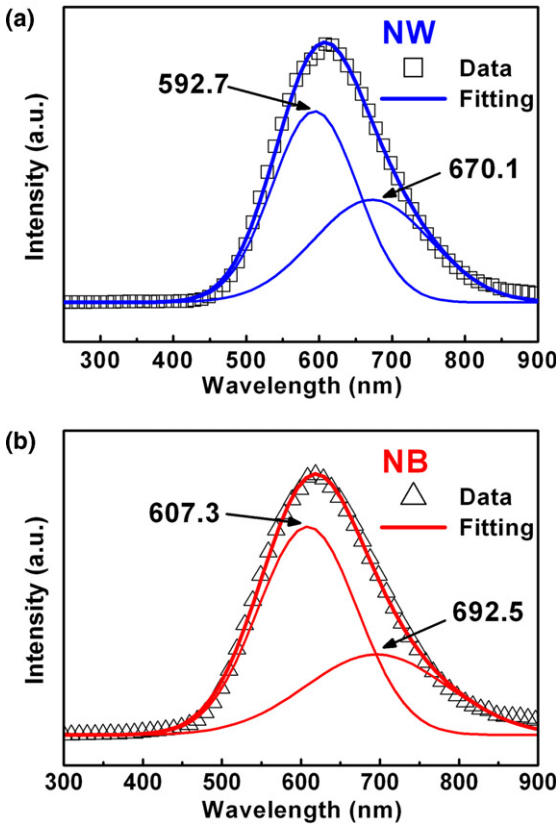

Figure 6. RT PL spectra of (a) the SnO_2 NWs (sample # 1) and (b) the SnO_2 NBs (sample # 6). Both original data (symbols) and double-peak Gaussian fittings (lines) are shown.

experiments with MnO_2 or MgO, instead of TiO_2, added to the source powder. These two compounds have distinct melting temperatures: MnO_2 decomposes at a low temperature of 535 °C, while MgO has a high melting point of 2832 °C. The same experimental parameters as in the growth of sample # 3 and sample # 4 were used. The SEM images taken on the growth products are shown in figures 5(c) and (d). In both cases, SnO_2 NWs with sizes similar to those in sample # 3 were observed, and there was no transition to NBs. The yields were much lower, indicating that the Sn vapor was reduced due to the dilution of Sn in the source.

We also investigated whether adding TiO_2 into the source powder (ZnO + graphite) can induce a similar morphology change in the ZnO NW growth. The experimental conditions were similar to those used in a previous report [48]. As shown in figures 5(e) and (f), adding TiO_2 into the source powder lowered the NW density and reduced their diameters. Therefore, the morphology change of SnO_2 nanomaterials from NW to NB induced by Ti is not a general effect for other combinations of transition metals and oxides. For a particular nanomaterial, the doping element must be carefully selected in order to induce the surface energy modification and the desired morphology change.

3.4. Comparative PL, Raman, and FE studies

The reliable control of the morphologies of SnO_2 allows us to carry out a systematic and comparative investigation on their physical properties. We compared the PL and FE characteristics of SnO_2 NWs and NBs because these properties are expected to depend on the morphology. In the RT PL spectra shown in figure 6, a broad peak at ∼600 nm (2.06 eV) was observed in both samples. Similar results have been reported before, and this peak was believed to originate from the defect-related electronic states in the band gap [27, 29]. The radiative interaction between the surface oxygen vacancies and the interfacial tin vacancies leads to the orange emission. For both NWs and NBs, the broad emission can be well fitted with two Gaussian peaks, possibly suggesting that there exist two different types of radiation center. For the NWs, the two peaks are located at 592.7 and 670.1 nm. For the NBs, they are at 607.3 and 692.5 nm. The emission peaks of the NBs show small red shifts compared to those of the NWs, possibly due to the differences in their morphologies and sizes [26].

The RT Raman spectra taken on NW and NB samples are shown in figure 7. Beside the characteristic Raman peak of the Si substrate at 519 cm^{-1}, three fundamental Raman scattering peaks were observed, at 478, 632, and 773 cm^{-1}. These peak positions are in good agreement with the previous results on a bulk crystal of rutile SnO_2 [61] and could be assigned to E_g, A_{1g}, and B_{2g} acoustic vibration modes, respectively. Compared with the NB sample, the NW Raman scattering shows a dramatic reduction of the A_{1g} peak and the B_{2g} mode is totally quenched. The size effect may have caused these modifications, and a similar trend was also observed

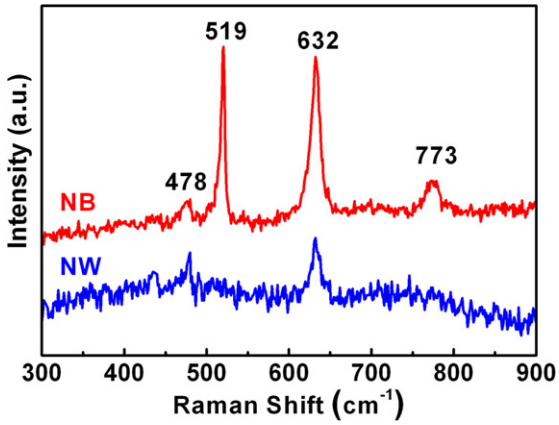

Figure 7. RT Raman scattering spectra of the SnO_2 NWs (sample # 1, lower curve) and the SnO_2 NBs (sample # 6, upper curve).

in the Raman spectra of SnO_2 nanoparticles with different sizes [62].

Figures 8(a) and (b) show the current density–electric field (J–E) curves in the FE measurements and the corresponding $\ln(J/E^2) - 1/E$ (Fowler–Nordheim, or FN) plots. The turn-on field, defined as the field required to reach a current density of 0.01 mA cm^{-2}, is ∼1.94 and ∼2.15 V μm^{-1} for NWs and NBs, respectively. Compared with NWs, NBs are capable of tolerating a much higher current density; the breakdown current of NBs is more than 30 times higher than that of the NWs. The better stability of NBs is possibly due to their larger cross-section areas and their lower resistance. The FN plots of both samples roughly follow straight lines, indicating that the FE currents can be attributed to the E-field-induced tunneling of electrons from the material surfaces into vacuum through a potential barrier [63, 64]. According to the FN law, the relation between the current density J and the applied field E can be depicted as $J = (A\beta^2E^2/\Phi)\exp(-B\Phi^{3/2}/\beta E)$, where Φ is the work function, A and B are constants with values of 1.54×10^{-6} A eV V^{-2} and 6.83×10^9 eV$^{-3/2}$ V m^{-1}, respectively, and β is the field enhancement factor. Assuming that the work function of SnO_2 is 4.5 eV [65], we estimated the β values of the NWs and NBs to be 1419 and 2253, respectively. Compared to the previous results [29, 43, 45, 66–68], the low turn-on fields and the high β values suggest good FE performances of the synthesized 1D SnO_2 nanomaterials.

4. Conclusions

In summary, we have achieved a reliable morphology control of SnO_2 NWs and NBs by selectively adding TiO_2 into the source powder during the vapor transport growth. In addition, by adjusting the oxygen content in the carrier gas and the geometry of the experimental setup, we were able to tune the SnO_2 NW diameters from ∼15 to ∼115 nm and the NB width from ∼30 nm to ∼2 μm. Although the Ti doping level is lower than the detection limits of our experimental tools, we propose the doping-induced surface energy modifications as the origin of the morphology transformation. RT PL, Raman, and FE measurements were carried out on the SnO_2 NWs and NBs,

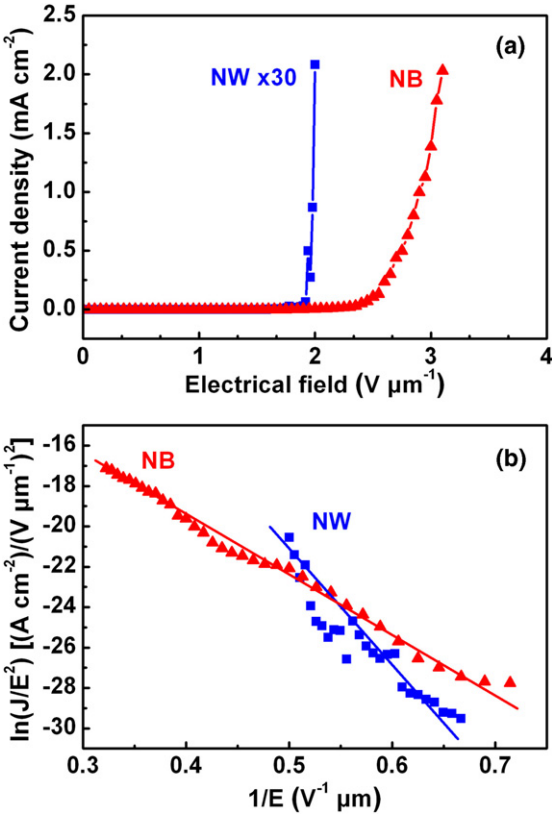

Figure 8. (a) Field emission J–E plots of the SnO_2 NWs (sample # 1, square symbols) and the SnO_2 NBs (sample # 6, triangle symbols). The current density of the NWs is multiplied by a factor of 30. (b) Corresponding FN plots.

and the results indicate that the physical properties sensitively depend on their different morphologies. In the future, tools with higher sensitivity such as synchrotron-based techniques should be used to unambiguously determine the Ti doping density, which will help to achieve a thorough understanding of the growth mechanism. Furthermore, quantitative theoretical modeling may guide us to select the appropriate doping elements to achieve the desired morphologies for certain host materials. The synthesis strategies reported here may be applied to other material systems to achieve reliable control of the shape and the size of nanomaterials.

Acknowledgments

The authors acknowledge research grant MOE RG 46/07 and Institute of Materials Research and Engineering for support.

References

[1] Pan Z W, Dai Z R and Wang Z L 2001 *Science* **291** 1947
[2] Dattoli E N, Wan Q, Guo W, Chen Y B, Pan X Q and Lu W 2007 *Nano Lett.* **7** 2463
[3] Hernandez-Ramirez F *et al* 2006 *Nanotechnology* **17** 5577
[4] Kolmakov A, Zhang Y X, Cheng G S and Moskovits M 2003 *Adv. Mater.* **15** 997
[5] Arnold M S, Avouris P, Pan Z W and Wang Z L 2003 *J. Phys. Chem.* B **107** 659

[6] Law M, Kind H, Messer B, Kim F and Yang P D 2002 *Angew. Chem. Int. Edn* **41** 2405
[7] Kolmakov A, Klenov D O, Lilach Y, Stemmer S and Moskovits M 2005 *Nano Lett.* **5** 667
[8] Wan Q, Huang J, Xie Z, Wang T H, Dattoli E N and Lu W 2008 *Appl. Phys. Lett.* **92** 102101
[9] Chen X H and Moskovits M 2007 *Nano Lett.* **7** 807
[10] Comini E, Faglia G, Sberveglieri G, Pan Z W and Wang Z L 2002 *Appl. Phys. Lett.* **81** 1869
[11] Hu J Q, Ma X L, Shang N G, Xie Z Y, Wong N B, Lee C S and Lee S T 2002 *J. Phys. Chem.* B **106** 3823
[12] Beltran A, Andres J, Longo E and Leite E R 2003 *Appl. Phys. Lett.* **83** 635
[13] Lee J S, Sim S K, Min B, Cho K, Kim S W and Kim S 2004 *J. Cryst. Growth* **267** 145
[14] Ying Z, Wan Q, Song Z T and Feng S L 2004 *Nanotechnology* **15** 1682
[15] Kalinin S V, Shin J, Jesse S, Geohegan D, Baddorf A P, Lilach Y, Moskovits M and Kolmakov A 2005 *J. Appl. Phys.* **98** 044503
[16] Huang H, Tan O K, Lee Y C, Tse M S, Guo J and White T 2006 *Nanotechnology* **17** 3668
[17] Zhou J X, Zhang M S, Hong J M and Yin Z 2006 *Solid State Commun.* **138** 242
[18] Huang J, Lu A X, Zhao B and Wan Q 2007 *Appl. Phys. Lett.* **91** 073102
[19] Hernandez-Ramirez F, Tarancon A, Casals O, Arbiol J, Romano-Rodriguez A and Morante J R 2007 *Sensors Actuators* B **121** 3
[20] Wang W Z, Xu C K, Wang G H, Liu Y K and Zheng C L 2002 *J. Appl. Phys.* **92** 2740
[21] Xu C K, Zhao X L, Liu S and Wang G H 2003 *Solid State Commun.* **125** 301
[22] Liu Z Q, Zhang D H, Han S, Li C, Tang T, Jin W, Liu X L, Lei B and Zhou C W 2003 *Adv. Mater.* **15** 1754
[23] Hu J Q, Bando Y, Liu Q L and Golberg D 2003 *Adv. Funct. Mater.* **13** 493
[24] Cheng B, Russell J M, Shi W S, Zhang L and Samulski E T 2004 *J. Am. Chem. Soc.* **126** 5972
[25] Sun S H, Meng G W, Wang Y W, Gao T, Zhang M G, Tian Y T, Peng X S and Zhang L D 2003 *Appl. Phys.* A **76** 287
[26] Luo S H, Fan J Y, Liu W L, Zhang M, Song Z T, Lin C L, Wu X L and Chu P K 2006 *Nanotechnology* **17** 1695
[27] Luo S H, Chu P K, Liu W L, Zhang M and Lin C L 2006 *Appl. Phys. Lett.* **88** 183112
[28] Yang M R, Chu S Y and Chang R C 2007 *Sensors Actuators* B **122** 269
[29] He J H, Wu T H, Hsin C L, Li K M, Chen L J, Chueh Y L, Chou L J and Wang Z L 2006 *Small* **2** 116
[30] Sun S H, Meng G W, Zhang G X, Gao T, Geng B Y, Zhang L D and Zuo J 2003 *Chem. Phys. Lett.* **376** 103
[31] Ma X L, Li Y and Zhu Y L 2003 *Chem. Phys. Lett.* **376** 794
[32] Dai Z R, Pan Z W and Wang Z L 2001 *Solid State Commun.* **118** 351
[33] Chen Y Q, Cui X F, Zhang K, Pan D Y, Zhang S Y, Wang B and Hou J G 2003 *Chem. Phys. Lett.* **369** 16
[34] Chen Y, Campbell L and Zhou W L 2004 *J. Cryst. Growth* **270** 505
[35] Ling C, Qian W Z and Wei F 2005 *J. Cryst. Growth* **285** 49
[36] Calestani D, Zha M, Zappettini A, Lazzarini L, Salviati G, Zanotti L and Sberveglieri G 2005 *Mater. Sci. Eng.* C **25** 625
[37] Orlandi M O, Leite E R, Aguiar R, Bettini J and Longo E 2006 *J. Phys. Chem.* B **110** 6621
[38] Yang R S and Wang Z L 2006 *J. Am. Chem. Soc.* **128** 1466
[39] Nguyen P, Ng H T and Meyyappan M 2005 *Adv. Mater.* **17** 1773
[40] Wang J X *et al* 2004 *Solid State Commun.* **130** 89
[41] Wang B, Yang Y H, Wang C X and Yang G W 2005 *J. Appl. Phys.* **98** 073520
[42] Budak S, Miao G X, Ozdemir M, Chetry K B and Gupta A 2006 *J. Cryst. Growth* **291** 405
[43] Wang Q Y, Yu K and Xu F 2007 *Solid State Commun.* **143** 260
[44] Dai Z R, Gole J L, Stout J D and Wang Z L 2002 *J. Phys. Chem.* B **106** 1274
[45] Zhang Y S, Yu K, Li G D, Peng D Y, Zhang Q X, Hu H M, Xu F, Bai W, Ouyang S X and Zhu Z Q 2006 *Appl. Surf. Sci.* **253** 792
[46] Wang B, Yang Y H, Xu N S and Yang G W 2006 *Phys. Rev.* B **74** 235305
[47] Lilach Y, Zhang J P, Moskovits M and Kolmakov A 2005 *Nano Lett.* **5** 2019
[48] Zhang Z, Wang S J, Yu T and Wu T 2007 *J. Phys. Chem.* C **111** 17500
[49] Zakrzewska K, Radecka A, Przewoznik J, Kowalski K and Czuba P 2005 *Thin Solid Films* **490** 101
[50] Carotta M C *et al* 2008 *Sensors Actuators* B **130** 38
[51] Kar S, Biswas S and Chaudhuri S 2005 *Nanotechnology* **16** 3074
[52] Khan A, Jadwisienczak W M and Kordesch M E 2006 *Physica* E **35** 207
[53] Wang Q, Li G D, Liu Y L, Xu S, Wang K J and Chen J S 2007 *J. Phys. Chem.* C **111** 12926
[54] Ding Y and Wang Z L 2004 *J. Phys. Chem.* B **108** 12280
[55] Yuan T C and Virkar A V 1988 *J. Am. Ceram. Soc.* **71** 12
[56] Zhang Z *et al* 2008 *J. Phys. Chem.* C **112** 9579
[57] Fan H J *et al* 2006 *Nanotechnology* **17** S231
[58] Fan H J, Barnard A S and Zacharias M 2007 *Appl. Phys. Lett.* **90** 143116
[59] Huang L S, Pu L, Shi Y, Zhang R, Gu B X, Du Y W and Wright S 2005 *Appl. Phys. Lett.* **87** 163124
[60] Duan J H, Yang S G, Liu H W, Gong J F, Huang H B, Zhao X N, Zhang R and Du Y W 2005 *J. Am. Chem. Soc.* **127** 6180
[61] Peercy P S and Morosin B 1973 *Phys. Rev.* B **7** 2779
[62] Dieguez A, Romano-Rodriguez A, Vila A and Morante J R 2001 *J. Appl. Phys.* **90** 1550
[63] Fowler R H and Nordheim L W 1928 *Proc. R. Soc.* A **119** 173
[64] Forbes R G 2001 *Solid-State Electron.* **45** 779
[65] Szuber J, Czempik G, Larciprete R and Adamowicz B 2000 *Sensors Actuators* B **70** 177
[66] Chen Y J, Li Q H, Liang Y X, Wang T H, Zhao Q and Yu D P 2004 *Appl. Phys. Lett.* **85** 5682
[67] Wang B, Yang Y H, Wang C X, Xu N S and Yang G W 2005 *J. Appl. Phys.* **98** 124303
[68] Li L J, Zong F J, Cui X D, Ma H L, Wu X H, Zhang Q D, Wang Y L, Yang F and Zhao J Z 2007 *Mater. Lett.* **61** 4152